Available online at www.sciencedirect.com
SCIENCE DIRECT®
Thin Solid Films 514 (2006) 10 – 19
thin solid films
www.elsevier.com/locate/tsf

Single crystal CrN/ScN superlattice soft X-ray mirrors: Epitaxial growth, structure, and properties

J. Birch, T. Joelsson, F. Eriksson *, N. Ghafoor, L. Hultman

Department of Physics, IFM, Linköping University, SE-581 83 Linköping, Sweden

Received 29 September 2005; received in revised form 11 January 2006; accepted 7 February 2006
Available online 20 March 2006

Abstract

Single crystal CrN/ScN superlattice films with modulation periods of 1.64 nm were grown on MgO(001) substrates. By utilizing a magnetically enhanced plasma in the vicinity of the substrate and a negative substrate bias, ion/metal nitride flux ratios of 45 and 144 were achieved during deposition of CrN and ScN, respectively. The effects of ion energies in the range [16–58 eV] and substrate temperatures in the range [535–853 °C] on the composition, interface width, crystal quality, and microstructure evolution were investigated using elastic recoil detection analysis, hard X-ray reflectivity, X-ray diffraction, and transmission electron microscopy (TEM). Minimal interface widths of 0.2 nm = 1/2 nitride unit cell were achieved at a growth temperature of 735 °C and ion energies of 24 and 28 eV for CrN and ScN, respectively. Under these conditions, also an optimum in the crystal quality was observed for near stoichiometric composition of CrN and ScN. TEM confirmed a cube-on-cube epitaxial relationship for the system with CrN(001)//ScN(001)//MgO(001) and CrN[100]//ScN[100]//MgO[100]. Also, the layers were coherently strained to each other with no misfit dislocations, threading dislocations, surface cusps, voids or gas bubbles present. Higher ion energies or lower deposition temperatures gave over-stoichiometric films with poor superlattice modulation while higher growth temperatures yielded a decreased crystal quality, due to loss of N. As-deposited superlattices with only 61 periods exhibited an absolute soft X-ray reflectance of 6.95% at an energy of 398.8 eV (Sc *2p*-absorption edge) which is comparable to the performance of Cr/Sc. The compositional modulation and phase structure was stable during extended annealing at 850 °C, which is the highest thermal stability for an X-ray multilayer mirror. It is concluded that the ScN layers serve as effective diffusion barriers to hinder decomposition of the CrN layers and stabilize the pseudomorphic superlattice structure. Nanoindentation experiments showed that the hardness of the CrN/ScN superlattice films was 19 GPa.

Keywords: CrN; ScN; Superlattice; X-ray mirrors; Reactive magnetron sputtering

1. Introduction

Multilayer optics have gained a large interest during the last decade, since the demand on mirror based optics has risen as the wavelength used in, e.g., lithography is getting close to the extreme ultraviolet and soft X-ray region ($\lambda = 1$–20 nm). Previously, amorphous multilayers of pure metallic Sc and Cr with <1 nm layer thickness have proven to be the most successful material combination for high reflectance soft X-ray mirrors in the wavelength range 2.4–4.4 nm, the so-called water window [1–6]. However, since the Cr/Sc multilayers are thermally unstable over 300 °C [7] they are not suited for operation in harsh environments such as in a free electron laser optical cavity or elevated temperature ambient. Also, as they are expected to be very sensitive to mechanical wear regular maintenance such as removal of debris by wiping may be impossible. However, ScN and CrN have relatively high thermal and mechanical stability which implies that they are good alternatives to Cr/Sc multilayers where the optical elements are subject to excess radiation, thermal, and/or mechanical loads. Transition metal superlattices and multilayers have been proven to be good candidates for applications in tough demanding environments. Nanometer scaled superlattices and multilayers composed of transition metal nitrides, e.g., TiN, VN, CrN, ZrN, NbN, and TaN have been widely studied due to the superhardening effect [8]. Hardness enhancement up to 2.5 times higher than the individual constituents have been reported when the compositional modulation period, Λ, is in the nm range [9,10]. These novel materials have found their

* Corresponding author.
E-mail address: freer@ifm.liu.se (F. Eriksson).

0040-6090/$ - see front matter © 2006 Elsevier B.V. All rights reserved.
doi:10.1016/j.tsf.2006.02.011

applications as hard coatings on cutting tools with very good resistance against wear at high temperatures [11]. However, until now, the transition metal ScN has been neglected in such nanolaminate applications. This is despite the fact that Sc is predicted to have the largest gain in energy upon forming a nitride among the transition metals and should thus be a candidate material for high hardness coatings. In fact, the hardness of single-crystal ScN films is 21 GPa [12], which is similar to that of TiN (21 GPa) [13]. ScN is now also gaining in interest due to its semiconducting properties (E_g=2 eV) [14]. The possibility to use it in lattice matched heterostructure devices as well as ohmic contacts with the group III-N semiconductors InN, GaN, and AlN have been proposed.

CrN, which is well documented as a hard coating [15] with a hardness of 28 GPa for epitaxial films, has also recently been shown to exhibit semiconducting properties with a vanishing density of states at the Fermi level [16]. Therefore, heterostructures and superlattice structures of ScN and CrN are materials which can be expected to have interesting electrical as well as mechanical properties. Previously there have been reports on the growth of single crystal epitaxial ScN thin films onto MgO(001) using both ultra high vacuum reactive magnetron sputtering [12,17] and molecular beam epitaxy (MBE) [18,19]. MBE growth employed a substrate temperature of 800 °C. However, a deposition temperature of above 750 °C was reported to be required when additional kinetic energy was provided to the surface by means of a stimulating flux of nitrogen ions. Reported studies on CrN mainly deals with polycrystalline films, however recently some articles reporting epitaxial growth have been published, both produced by magnetron sputtering [15] and MBE [20]. The best-quality CrN films are obtained by reactive magnetron sputtering and with an assisting flux of kinetic nitrogen ions. However, it has been shown that the growth temperature must be kept below 700 °C in order to avoid decomposition to Cr_2N and N during film deposition [15]. As-deposited CrN films are also sensitive to thermal annealing above 550 °C as this leads to recrystallization and eventual nitrogen loss [21].

These non-overlapping temperature ranges for growth of ScN and CrN epitaxial films thus makes it a challenge to find deposition parameters that allows for sequential deposition of the hundreds of sub-nm layers that build up a superlattice. However, we suggest as a possibility that ultrathin epitaxial CrN layers can be pseudomorphically stabilized when grown on to single crystal ScN for temperatures higher than 700 °C. Likewise, the epitaxial growth temperature of ScN may be lowered by providing additional energy to the growing surface by means of increasing the flux of ions assisting the growth. In order not to cause crystalline defects and interfacial mixing in the superlattice, increased supply of kinetic energy should be provided by a *high flux of ions*, $J_{ion}/J_{Me}>20$, with a maintained *low* (10–30 eV) *kinetic energy per ion* [1].

Based on this approach, we here report on the realisation of single crystal CrN/ScN superlattice X-ray mirrors designed for 398.8 eV soft X-rays (Sc *2p*-absorption edge). The effects of different growth temperatures and ion assistance energies on the interface and crystal qualities, as well as impurity incorporation were investigated in detail by X-ray diffraction (XRD), hard X-ray reflectivity (HXR), transmission electron microscopy (TEM), and elastic recoil detection analysis (ERDA). For the optimal deposition conditions, based on the structural characterization, the performance of the CrN/ScN X-ray mirrors were investigated with respect to absolute near-normal soft X-ray reflectivity, thermal stability by high-temperature XRD, as well as mechanical hardness by nano indentation. The results are compared to state-of-the-art Cr/Sc and W/B_4C multilayer mirrors in order to investigate the feasibility of CrN/ScN superlattices as a more robust alternative.

2. Experimental details

CrN/ScN superlattice thin films were deposited by reactive magnetron sputter deposition in a dual cathode high vacuum system onto polished $10\times10\times1\,mm^3$ MgO(001) single crystal substrates. The size of the chamber is 500 mm in diameter and 350 mm in height with a standard background pressure of 2×10^{-7} Torr (2.67×10^{-5} Pa), obtained using a 310 l/s turbo molecular pump backed by a rotary vane pump. The substrate temperature, T_S, was measured by an optical pyrometer, using a wavelength of 1.1 μm, which was calibrated against a thermocouple. All substrates were pre-heated in vacuo at T_S=835 °C for 1 h in order to create a clean well ordered surface, and then T_S was decreased to 735 °C where a nucleation bilayer of 0.82 nm CrN and 0.82 nm ScN was deposited before setting the final deposition temperature and starting the deposition of the superlattices. The two 75 mm-diameter Cr (99.97%) and Sc (99.9%) sputtering targets were placed 125 mm above the substrate table, each at a line-of-sight 25° off the substrate surface normal. N_2 (99.9997%) at a pressure of 8 mTorr was used as a sputtering gas. The magnetron currents and voltages I_{Cr}=0.17 A, U_{Cr}=330 V, I_{Sc}=1.0 A, and U_{Sc}=285 V yielded the deposition rates r_{CrN}=0.236 Å/s and r_{ScN}=0.476 Å/s, as determined by X-ray reflectivity thickness measurements using the method of asymmetric superlattices [22]. The deposition fluxes from the sources were modulated by fast acting computer controlled shutters in front of each target. In order to attract ions from the nearby plasma, a negative substrate bias, V_S, was applied during growth. In this work, the effects of V_S in the range [−60 V<V_S<V_F] (V_F denotes the floating potential) and, T_S in the range [535 °C<T_S<835 °C] was studied.

Two series of CrN/ScN superlattices were produced. Both series were designed with N=61 repetitions of a modulation period Λ=1.7 nm and equal individual layer thicknesses ($D_{CrN}=D_{ScN}$ or $\Gamma=D_{ScN}/\Lambda=0.5$). In the first series the deposition temperature, T_s, was varied (535, 635, 735 and 835 °C) and with no ion assistance. In the second series all depositions were performed at 735 °C, as determined from the results of the first series as well as other depositions not presented here, but with an ion assistance in the average ion energy range between 17 and 45 eV, as determined by flat probe measurements.

The magnetic configuration in the chamber was such that the magnetic fields from the unbalanced (type II) [23,24]

magnetrons were of opposing polarity, closing the strong B-fields from the outer ring poles just above the substrate. An in-situ solenoid, with a coil current of 5 A created an axial magnetic field which coupled to the magnetic field from one the magnetron producing a field strength of $B=10$ mT perpendicular to the substrate surface. By reversing the coil current in-between each layer, the solenoid field was at all time coupled with the magnetron source being used for deposition throughout the superlattice growth [25]. Plasma characterisation in the region [$-50\,V<V_S<-20\,V$] was carried out using an electrostatic Langmuir probe (tungsten wire, 4 mm long, 0.2 mm diam.) and in the range [$-80\,V<V_S<-20\,V$] using a circular flat probe (stainless steel, 1.77 mm^2) positioned at the sample position.

The crystal quality was characterized using X-ray diffraction. Symmetric (θ–2θ) overview scans were performed using a Philips Bragg–Brentano diffractometer equipped with separate θ and 2θ drives, and a line focus Cu K_α lab-source. The layer thicknesses and interface quality of the superlattice structures were characterized by specular hard X-ray reflectivity combined with HXR simulations. The HXR curves were measured using the same setup as the XRD measurements. The HXR simulations were performed using the PCGIXA software which takes dynamical effects as well as effects of absorption and refraction into account [26].

In order to establish the stability of the X-ray mirrors at elevated temperature, XRD as well as HXR was performed in-situ during isochronal annealing for at least 24 h at successively higher temperatures up to 900 °C, starting from ambient. Up to 700 °C the temperature was raised in steps of 100 °C, where after the increase between each temperature was 50 °C. The measurements were performed in a Büehler HDK 2.4 high temperature high vacuum chamber with a Be-window, fitted to a Philips X'pert θ–θ MPD diffractometer with the same X-ray optical configuration as the Bragg–Brentano diffractometer.

The concentrations of nitrogen as well as carbon, oxygen, and fluorine impurities were determined to an accuracy of <0.3% by Elastic Recoil Detection Analyses of the as-grown superlattices using a 35 MeV Cl^{7+} ion beam at a grazing incident angle of 10° [27]. As a side effect, the metal concentration could be determined simultaneously by analyzing the energy loss of the scattered Cl-ions. However, the mass resolution above $Z=10$ was not sufficient to allow for separation of Sc and Cr.

Microstructure and layer definition was studied in cross-sectional transmission electron microscopy (XTEM) using a Philips CM20 UT instrument with a LaB_6 filament and an acceleration voltage of 200 kV. The cross-sectional samples were prepared using a low energy ion-beam milling method.

The X-ray mirror performance at 398.8 eV radiation (3.115 nm wavelength) was characterized by absolute near-normal incidence soft X-ray reflectivity. The measurements were performed in the BESSY polarimetry chamber using the synchrotron radiation beamline UE56/1 at BESSY II.

Mechanical properties of the films were determined by nanoindentation using a Hysitron Indentor equipped with a Berkowich diamond tip. In order to keep the indentation depth shallow compared to the film thickness maximum loads of 500 μN were applied to the sample. The Oliver and Pharr approach [28] was used to extract values of hardness and Young's modulus from the load–displacement data.

3. Results and discussion

The Langmuir plasma probe measurements at the substrate position revealed plasma potentials V_P of $V_{P,CrN}=-22$ V and $V_{P,ScN}=-28$ V for CrN and ScN, respectively. The energies of the ions attracted to the substrate, $E_{Ion,CrN}$ and $E_{Ion,ScN}$, given by $E_{Ion}=|V_S-V_P|$ eV are thus, contrary to common sputtering situations, considerably lower than the applied substrate bias potential. The unusually high *negative* values are a consequence of a considerable amount of secondary electrons from the magnetrons that are guided by the magnetic field to the substrate region where they, in turn, ionize the nitrogen sputtering gas. The majority (>95%) of the ions can be expected to be N_2^+ as has been shown for deposition of TiN under similar conditions [29]. The injection of a high flux of electrons towards the substrate also manifested itself in unusually high negative values of the floating potentials V_F, which were determined to $V_{F,CrN}=-38$ V and $V_{F,ScN}=-46$ V for CrN and ScN, respectively. Thus, even at floating substrate potential, the growing film was subject to fluxes of ions with energies $E_{Ion,CrN}=16$ eV and $E_{Ion,ScN}=18$ eV, during CrN and ScN deposition, respectively. The flat probe measurements showed that the ion-to-neutral arrival flux ratios, Φ, (i.e., the number of nitrogen ions per nitride formula unit arriving at the substrate) were $\Phi_{CrN}=42$ ions/CrN and $\Phi_{ScN}=144$ ions/ScN. Typically flux ratios for balanced and unbalanced magnetron sputtering of metals without a coupling coil are $\Phi\sim0.1$ and $\Phi\sim1$, respectively. The sputtering conditions used in this work thus provide considerably higher relative ion fluxes than what is normally possible using magnetron sputtering without a coil arrangement. The high ion flux values are a consequence of the combined effect of the extended plasma and the low sputtering yield of the nitrides, which in turn results in low deposition rates.

ScN can be sputter deposited epitaxially, with a cube-on-cube relationship, onto MgO(001) films and have been reported to have the best crystal quality using $\Phi_{ScN}=14$ and $E_{Ion,ScN}=20$ at a substrate temperature of 750 °C [12,17]. However, if the energy of the ions assisting the growth was raised to 50 eV, ion-induced damage with N_2 gas bubbles and large compressive stresses were reported to evolve in the films. At temperatures higher than 750 °C there is a risk of spinel formation between the film and substrate components. On the other hand, ion assisted sputter deposition of epitaxial single films of CrN onto MgO(001) have been reported using $\Phi_{CrN}=6$–14, and $E_{Ion,CrN}=12$ eV, at substrate temperatures below 700 °C [15]. Above 700 °C, under-stoichiometric CrN_x ($x<1$) films are formed due to decomposition of CrN to Cr_2N and desorption of N [15,34–36]. The ion fluxes in this work are thus about 10–100 times higher than those used previously for ion assisted epitaxy of single films. That offers a route to growth of ScN/CrN superlattices since the corresponding enhancement of adatom mobility and N activity allow for a further reduction of the

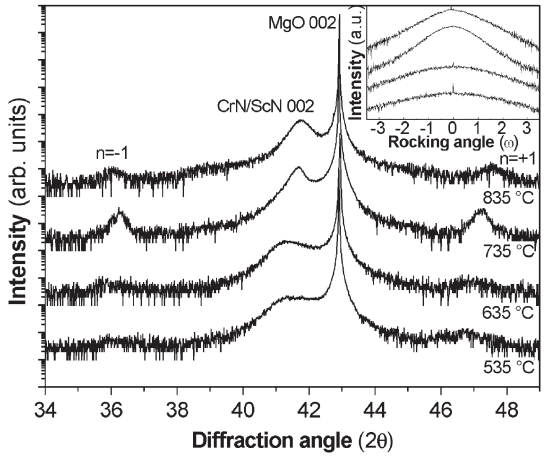

Fig. 1. Overview XRD θ–2θ scans over the average CrN/ScN 002 Bragg peak as well as the first orders ($n=\pm1$) superlattice satellites from films synthesized at four different growth temperatures (535, 635, 735, and 835 °C) using a floating substrate potential. The inset shows the ω-rocking curves over the Cr/ScN 002 peak for the same superlattices arranged in the same order as in the main figure.

epitaxial temperature of ScN to a common temperature where epitaxial CrN can be expected to form.

XRD and HXR measurements were conducted on each grown superlattice directly after the deposition. Based on immediate analyses of superlattice period Λ, intensities of the reflectivity peaks, and the definition of the diffraction peaks, a fast feedback loop for process optimization was achieved.

In order to investigate how the crystal quality of the CrN/ScN superlattices was influenced by the growth temperature as well as the ion assistance energy, XRD was performed over the superlattice CrN/ScN 002 average Bragg peak as well as the accompanying superlattice ±1 order satellites on each sample. Fig. 1 shows overview θ–2θ scans and the inset shows ω scans of the CrN/ScN 002 peaks from superlattices grown at different substrate temperatures, T_S, in the range [535–835 °C], with the lowest ion energies, $E_{Ion,CrN}=16$ eV and $E_{Ion,ScN}=18$ eV, in our experiment. As can be seen in the θ–2θ scans as well as the ω scans, the average CrN/ScN 002 Bragg peak, which reflects the quality of the crystalline lattice in the sample, is best defined in terms of intensity as well as width for the superlattice grown at $T_S=735$ °C. The $n=\pm1$ superlattice satellites exhibit the same qualitative behaviour with a clear optimum at the same temperature. The CrN/ScN Bragg peak position corresponds to an average crystal lattice parameter in the growth direction of $\bar{c}=0.432$ nm. The good agreement with a theoretical average lattice parameter of 0.4321 nm, which can be calculated by the expression $\bar{c}=(D_{CrN}c_{CrN}+D_{ScN}c_{ScN})/\Lambda$, assuming equally thick layers according to the design and using bulk unstrained lattice parameters ($c_{CrN}=a_{0,CrN}=0.4140$ nm, $c_{ScN}=a_{0,ScN}=0.4501$ nm), indicates that the superlattice is close to the design with $\Gamma=0.5$ and consisting of near-stoichiometric CrN and ScN components. We can therefore conclude that for the low ion assistance energies $E_{Ion,CrN}=16$ eV and $E_{Ion,ScN}=18$ eV, the overall crystal perfection in the superlattice as well as the definition of the superlattice layering is highest when we used a growth temperature of 735 °C. The decrease and broadening of the Bragg peaks is accompanied by a shift to lower 2θ angles when lower T_S were used, showing that the average crystal lattice becomes less ordered and expanded at lower growth temperatures. Also at the higher temperature 835 °C, a lower and broader Bragg peak indicates less structural order on an atomic level. However, the peak is shifted towards higher angles, indicating that the average lattice parameter decreased. No sign of Cr_2N peaks could be found in any of the diffraction patterns.

Fig. 2 shows a HXR scan from a CrN/ScN superlattice film with $\Lambda=1.7$ nm along with the corresponding WINGIXA HXR simulation. Superlattice reflectivity peaks up to the third order ($n=3$) can be seen at angles up to $2\theta=8°$ which are characteristic of the best superlattices in this work. As can be seen, the peaks are well defined without any broadening with increasing order n which shows that the superlattice constitutes of flat layers without any lateral or transverse layer thickness variations. The Kiessig fringes that are visible up to θ values of about 3°, which is above the first order ($n=1$) superlattice peak, are also significant for a multilayered structure with high long range layer conformity. By fitting model HXR simulations to the experimental data, quantitative analyses of the interface roughness and individual layer thickness were made. The best fit model simulation in this example yielded $N=61$ bi-layers with individual layer thickness of $D_{CrN}=0.763$ nm and $D_{ScN}=0.972$ nm ($\Gamma=D_{CrN}/\Lambda=0.44$) and interface widths of $\sigma=0.18$ nm (1 monolayer). It can be noted that the measured Λ is very close to the designed bilayer thickness while Γ is somewhat smaller than the nominal value of 0.5. This is a reflection of the difficulties in maintaining constant deposition rates over several weeks of depositions while it is easy to maintain the bilayer period constant during the entire time frame of the project through continuous feedback from direct measurements of Λ by HXR and XRD. A minor part of the discrepancy in Γ may be due to coherency lattice strains

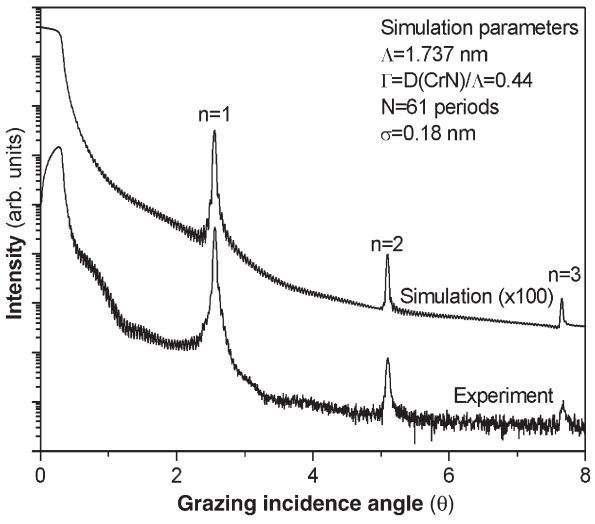

Fig. 2. Hard X-ray reflectivity (HXR) scans from an epitaxial (002) oriented CrN/ScN superlattice film grown at $T_S=735$ °C on MgO(001) substrate with ion assistance energies of $E_{Ion,CrN}=24$ and $E_{Ion,ScN}=28$ eV (lower curve) and simulated HXR (top curve).

that act to contract the CrN and expand the ScN layers. Such a behaviour is expected when an epitaxial superlattice consists of sub-nm individual layers due to the Poisson reactions to the lateral lattice mismatch strains. However, even in a fully strained coherent superlattice, the effect would not exceed ±4.5% contraction or expansion. However, in practice for the synthesis of soft X-ray CrN/ScN superlattice mirrors the Γ-value is not critical as the peak reflectivity dependence on the value of Γ does not vary significantly between $0.4 < \Gamma < 0.6$.

The number of HXR peaks and their absolute intensities are directly related to the average abruptness of the chemical profiles at the interfaces. By studying the evolution of the intensities of the different orders HXR peaks ($n = 1$ to 3) when the superlattices were grown under different conditions, qualitative conclusions regarding the perfection of the superlattices could be drawn. The peak intensities of the HXR peaks from superlattices grown at different substrate temperatures T_S with ion assistance energies $E_{Ion,CrN} = 16$ eV and $E_{Ion,ScN} = 18$ eV exhibited a clear plateau between 635 °C and 735 °C with a slightly higher intensity at the high temperature side. The peak intensities from superlattices grown at 735 °C but with varied ion assistance energies had a clear maximum at ion energies of $E_{Ion,CrN} = 24$ eV and $E_{Ion,ScN} = 28$ eV. Films grown at 535 °C and 635 °C, and 853 °C with different ion energies always exhibited considerably lower peak intensities than those grown at $T_S = 735$ °C with $E_{Ion,CrN} = 24$ eV and $E_{Ion,ScN} = 28$ eV. Additional superlattice mirrors were then synthesized under these optimal conditions for further characterization of their properties.

Cross-sectional TEM was employed to study the microstructural evolution in the films and the occurrence of any growth defects. Fig. 3 shows the typical results from one as-deposited superlattice mirror sample which was grown at the optimal combination of temperature ($T_S = 735$ °C) and ion assistance energy ($E_{Ion,CrN} = 24$ eV and $E_{Ion,ScN} = 28$ eV). The superlattice contained 61 bilayers of modulation period $\Lambda = 1.7$ nm, and interface widths of $\sigma = 0.18$ nm according to XRD and HXR measurements.

As can be seen in Fig. 3(a), the structure has defined layering and is free from defects such threading dislocations, surface cusps, voids, or gas bubbles. The contrast due to the CrN/ScN layers appears to be meanderings along the lateral direction. This, however, is likely an artifact from the sample preparation and any inhomogeneous relaxation in the thin XTEM sample, since neither HXR nor XRD would show any appreciable superlattice peaks from such a structure. The layer thicknesses in this sample are only 0.85 nm which are much thinner than the extension of contrast due to lattice strain fields such as those that can be observed in the substrate at the interface to the superlattice. Likely reasons for the meandering contrast in the TEM image are thus interference between strain fields and lattice mismatch corrugation of the sample wedge due to large internal stresses. The single-crystal structure of the superlattice is confirmed by the selected area electron diffraction pattern in Fig. 3(b), where superlattice satellite peaks of the first order are visible. The expected cube-on-cube epitaxial relationship CrN (001)//ScN(001)//MgO(001) and CrN[100]//ScN[100]//MgO [100] is also confirmed by this pattern. From the lattice-resolved image in Fig. 3(c) the atomic ordering reveals that the CrN and ScN layers are coherently grown on top of each other. Although the lattice planes are undulating in the same fashion as the superlattice layers in Fig. 3(a), no misfit dislocations can be seen in the images.

In order to reveal eventual incorporation of impurities, which can be detrimental for the soft X-ray reflectivity, and to confirm the formation of stoichiometric nitride layers, ERDA were performed on the superlattices.

N and metal concentrations by ERDA and energy loss spectroscopy of the Cl ions yielded an atomic density in the

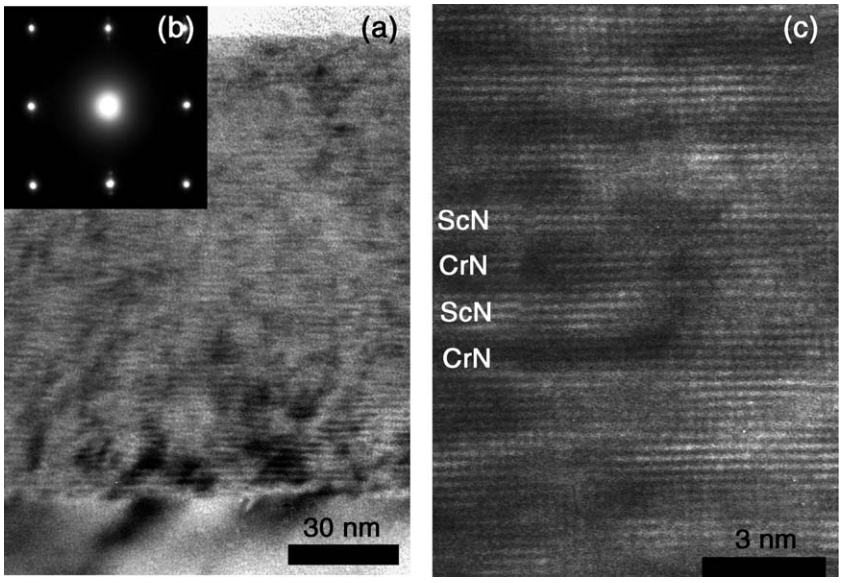

Fig. 3. Cross-sectional TEM micrograph from a CrN/ScN superlattice with the modulation period Λ of 1.7 nm and interface widths σ of 0.18 nm grown at 735 °C with ion assisting energies $E_{Ion,CrN} = 24$ eV and $E_{Ion,ScN} = 28$ eV; (a) overview, (b) selected area electron diffraction pattern obtained along the MgO [010] zone axis, and (c) high-resolution image.

superlattices of $1.10 \pm 0.04 \times 10^{23}$ cm^{-3} independent of deposition parameters. This is about 10% higher than what would be expected from pure films with bulk densities. This condition is likely different from other CrN and ScN epitaxial film growth experiments by reactive magnetron sputtering with similar ion energy ranges, but with much lower ion fluxes, where instead bulk density is inferred. Due to the limited mass resolution of the energy loss spectroscopy of the Cl-ions, however, the relative concentrations of Cr and Sc could not be extracted.

Fig. 4 shows the film compositions as determined by ERDA. First, the impurity levels of O, F, and C are shown to increase as the growth temperature is increased (see Fig. 4(a)). The occurrence of fluorine in the films indicates that residues of fomblin pump oil, which was used in the pumping system, might have been present in the deposition chamber. Fomblin oils are very stable and are based on perfluoropolyether and thus contain significant amounts of F, C, and O. However, at the elevated substrate temperatures used in this work, the hydrocarbons are easily cracked on the growing film surface such that the cracking products may be incorporated into the film. Although fomblin oil contains oxygen, the proportional amounts of O and C found in the films are too high in order to originate solely from eventual oil residues. Additional sources of these elements are O_2, H_2O, CO_2, and CO that are common residual gases in high vacuum chambers. The observed increased amounts of incorporated impurities as T_S was increased, is due to considerable thermal desorption of residual gases from the chamber walls. This was also reflected in the base pressure of the chamber, which typically increased by one order of magnitude as T_S was increased from room temperature to 835 °C.

More interesting is to consider the nitrogen and metal concentration as a function of temperature (see Fig. 4(c) where the N/M nitrogen-to-metal concentration ratio also is given. At the lowest substrate temperature of 535 °C, films are very over-stoichiometric with an N/M = 1.23, which is seen to decrease to N/M = 1.03 as T_S is increased to 835 °C. These temperatures are the highest yet reported for growing single-phase CrN with $x \approx 1$. Previous reports have shown that the amount of nitrogen in Cr–N films was substantially reduced with increasing T_S such that sub-stoichiometric CrN_x ($x < 1$) and Cr_2N are deposited at $T_S \geq 700$ °C and essentially metallic Cr(N) films form at $T_S \approx 800$ °C [15]. The resulting N uptake is a competition between reaction for structural bonding or any implantation, and loss by recombination of N_2 formation followed by desorption during deposition. With the present

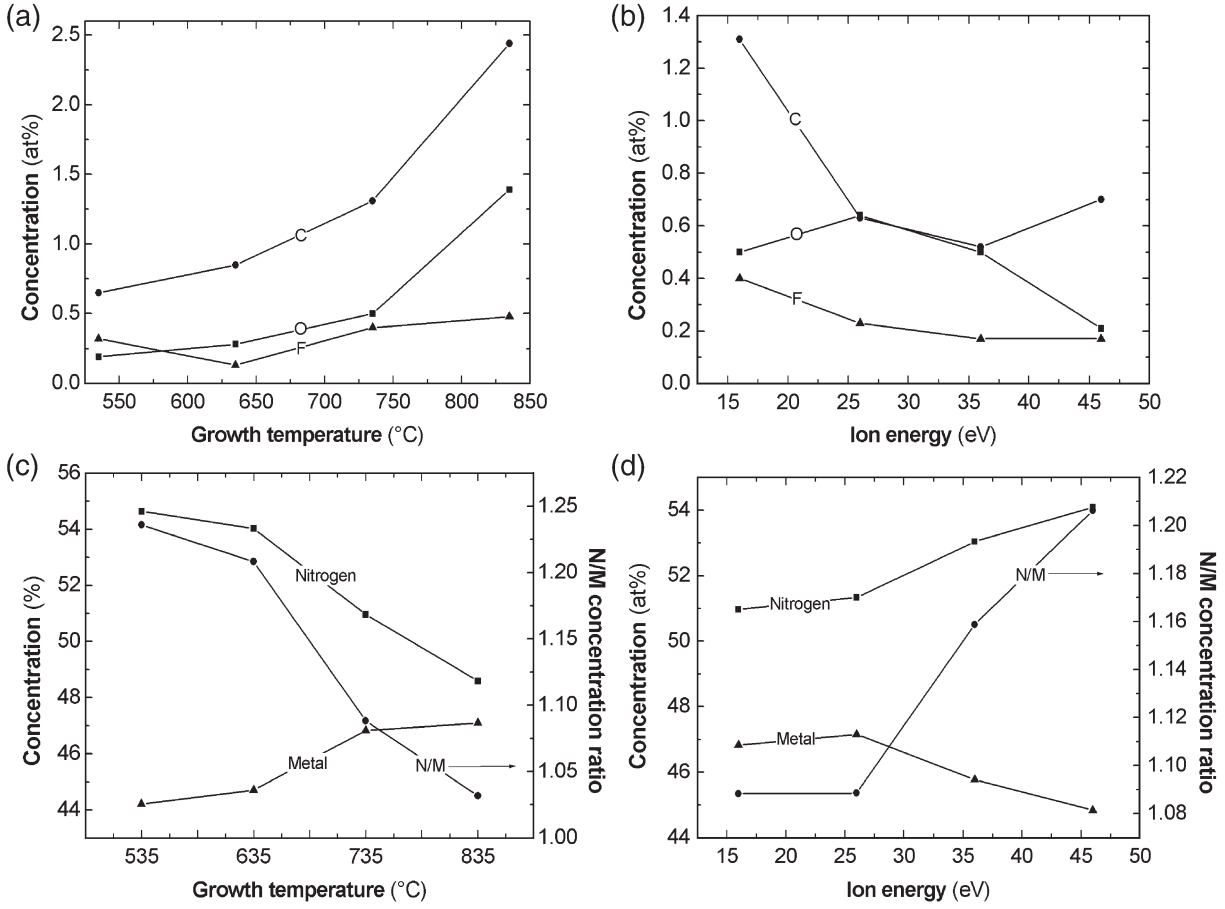

Fig. 4. Elemental concentrations in the superlattices. (a) The C, O and F impurity levels as a function of growth temperature at $E_{Ion,CrN} = 16$ eV and $E_{Ion,ScN} = 18$ eV ion energy, (b) the C, O and F impurity levels as a function of ion energy at substrate temperature 735 °C, (c) the nitrogen and metal concentrations as a function of growth temperature, and (d) the nitrogen and metal concentrations versus ion energy at $T_S = 735$ °C. Also the nitrogen-to-metal elemental ratios are given in figures (c) and (d). The energy scales show the average of the $E_{Ion,CrN}$ and $E_{Ion,ScN}$ weighted with respect to the ion fluxes.

deposition conditions, however, films grown at as high T_S as 825 °C had a retained cubic CrN phase structure. Before further discussing the apparent increase in N activity for the present CrN layers, we will consider the effect of ion energy on the N content.

The influence of ion energy on the composition of as-deposited films deposited at $T_S = 735$ °C is presented in Fig. 4 (d). The nitrogen content increased with increasing energy from slightly over-stoichiometric composition (N/M = 1.08) at floating potential to very over-stoichiometric, N/M = 1.20 at $E_i = 47$ eV. This effect can have different reasons, including more effective nitrogen uptake from a higher steady-state atomic N surface population due to collisionally induced dissociative chemisorption or from subplantation of N in the film surface during growth of both CrN and ScN layers. As mentioned above, the CrN layers have retained a significant amount of N at this high temperature. For ScN layers, however, deposition of ScN(001) films is reported to yield stoichiometric composition at $T_S = 750$ °C [12] when grown with ion-surface interactions in the same energy range as the present work. However, N trapping at non-lattice sites in over-stoichiometric epitaxial films and eventual supersaturation with precipitation of N_2 gas bubbles within the lattice was reported [12] although a moderate ion-to-metal flux ratio of $\Phi = 14$ was used, as compared to $\Phi_{ScN} = 144$ in this work.

For the impurity levels, Fig. 4(b) shows that the O and F contents become reduced significantly at ion energies over 25 eV and vanish effectively at $E_i \geq 47$ eV. The C content, however, exhibits an initial steep drop with increasing ion energy with a minimum around the intermediate ion energies, and then increases again for $E_i \geq 37$ eV. We ascribe the loss of F and O to ion-bombardment stimulated desorption during growth as the enthalpy of formation of the respective metal hydroxides and fluorides are lower than for the corresponding nitrides or carbides. The variation in C content can thus be associated with an initial desorption of hydrocarbons followed by stimulated carbide formation or recoil implantation of C into the lattice similar to what was discussed for the N-uptake above.

From the results this far, we conclude–however not in line with studies hitherto of CrN and ScN film deposition–that a narrow substrate temperature window of around $700 \leq T_S \leq 800$ °C exists for the deposition of stoichiometric CrN(001) and ScN(001) layers. The process presented here requires basically two conditions. Firstly, a high flux of low energy ions provides for N activation in the nitride formation, not the least important for the CrN layer, and recoil implantation of N to compensate for the concurrent N_2 desorption from the film surface during deposition. Second, the successive layering of CrN and ScN layers in the form of a superlattice supplies both a capping layer (ScN) to act as a diffusion barrier against N loss from the CrN that is allegedly instable at stoichiometric composition at these temperatures, but also a buffer layer (CrN) to accommodate any trapped N in otherwise over-stoichiometric ScN layers. In addition, we submit that the coherency strain from the pseudomorphic growth of the two nitrides in the form of a superlattice will fixate the N sublattice.

The performance of these CrN/ScN superlattices as normal incidence soft X-ray mirrors is crucially dependent on, not only a high structural perfection, but also a high purity of the layers as the scattering factor contrast between the layers strongly depends on the electron density and the absorption edges of the constituting elements. An impurity level of ~10% has been shown to reduce the absolute near-normal reflectance by a non-negligible amount [30,31]. However, the impurity levels encountered in our films grown under the optimum conditions are expected to influence the performance only marginally. In a similar way, the stoichiometry with respect to nitrogen and metal in the individual layers may have an influence by altering the X-ray contrast. However, the major cause of degradation of the soft X-ray reflectance is eventual interdiffusion between the extremely thin (0.85 nm) CrN and ScN layers. The previous HXR analyses showed that the interface width in our mirrors are only 0.18 nm wide. It is known, however, that grazing hard X-rays and normal incidence soft X-rays, due to their vastly different lateral and vertical coherence lengths, do not sense the same type of interface imperfections and it is therefore generally not possible to extrapolate the structural parameters from HXR analyses to predict the behaviour in the soft X-ray regime.

In order to characterize the soft X-ray mirror performance of the single crystal CrN/ScN superlattice mirrors, absolute near normal-incidence reflectivity measurements were performed with 398.8 eV ($\lambda = 3.115$ nm) X-rays corresponding to the Sc *2p* absorption edge where the reflectivity is expected to be maximum.

The solid line in Fig. 5 represents the experimental angular reflectivity data from an $N = 61$ periods superlattice grown at a temperature of $T_S = 735$ °C with $E_{Ion,CrN} = 24$ eV and 28 eV ion assistance. Although the mirror only contain 61 bi-layers, the peak reflectivity is as high as 7% at 63.25° and the curve exhibits clear Kiessig fringes, both indicative of a high lateral and transverse order in the layer structure. The dotted line in

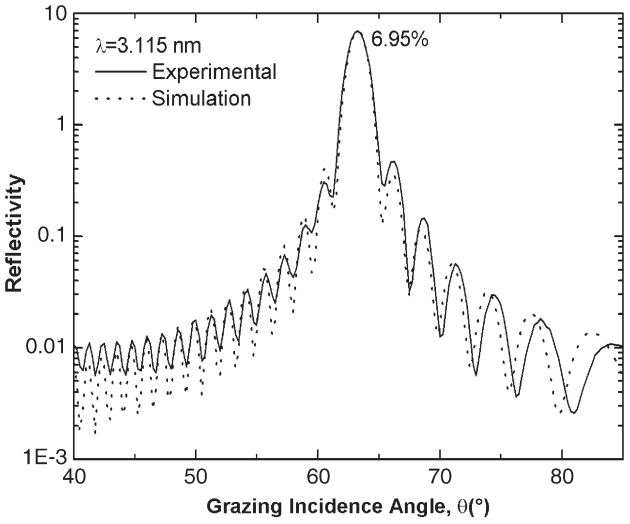

Fig. 5. Solid line: near normal-incidence soft X-ray reflectance measured at a wavelength of 3.115 nm showing a maximum of 6.95% at $\theta = 63.25°$. Dotted line: best fit IMD simulation of the reflectance. The simulation yielded a period of $\Lambda = 1.741$ nm and interface widths of $\sigma = 0.2$ nm.

Fig. 5 shows the best fit simulation by the IMD software [32] using optical constants for Cr, Sc, and N from Henke et al. [33] and assuming dense and stoichiometric CrN and ScN layers without any contamination. A superlattice model with periodicity $\Lambda = 1.741$ mm, layer thickness ratio $\Gamma = 0.5$, and interface widths $\sigma = 0.2$ nm was used and, as can be seen, yielded a very good fit to the experimental curve. The obtained interface width $\sigma = 0.2$ nm is in excellent agreement with the $\sigma = 0.18$ nm obtained from the HXR analyses. It means that the chemical gradient over the interfaces extends over only one-half CrN or ScN unit cell in the [001] direction indicating that the growth occur as in a layer by layer fashion. Since any epitaxial layer, grown with an arbitrary thickness corresponding to a non-integral number of monolayers, must be terminated with surface steps and/or 2-dimensional islands on the surface, the interface abruptness in our CrN/ScN superlattices equals what is theoretically possible. Only phase locked epitaxy, where the deposition can be terminated exactly upon completion of the last monolayer in each superlattice layer, can provide atomically abrupt interfaces. A small discrepancy of the Kiessig fringe frequency is observed above the main peak which is mostly influenced by the details of the Sc optical constants just above the *2p* absorption edge. We believe that the observed discrepancy is an artefact due to the lack of detail in the Henke data of Sc very close to the absorption edge. Also layers with densities differing significantly from the modelled bulk values could have a similar effect. However, this can be ruled out as a cause of the Kiessig fringe mismatch since our ERDA analyses showed a slight over-stoichiometry for this film and the overall atomic density was found to be 10% higher than expected from bulk values of CrN and ScN. It should also be pointed out that including more interdiffusion, intermixing, interface roughness or any impurity dilution of the layers would yield a lower simulated reflectivity and a poorer fit to the experimental data. These results show that both the performance and quality of the superlattices are well in par with the best metallic Cr/Sc soft X-ray multilayer mirrors [2,6,7,30,31].

In order to investigate the feasibility of using the CrN/ScN superlattice X-ray mirrors as highly stable optical components in demanding applications exerting a high load of radiation power on the mirrors, we performed XRD as well as HXR at elevated temperatures on a superlattice grown under the optimum conditions as determined by XRD and HXR. During 24 h isochronal annealing at each of the temperatures 500, 600, 700, 750, 800, and 850 °C, neither XRD nor HXR exhibited any changes indicating a very high thermal stability. It is interesting to note that the layers are intact above 850 °C at which temperature pure CrN is reported to decompose from under stoichiometric CrN_x to Cr_2N, Cr, and nitrogen [21,34–36]. However, such thermodynamically driven decomposition of the CrN layers can be hindered by the more thermally stable ScN layers in CrN/ScN multilayers or superlattices. Hence the ScN layers act as diffusion barriers and keep the Cr and N atoms in the δ-CrN lattice. We note from the TEM analyses that the CrN/ScN interfaces are epitaxial and coherently strained (see Fig. 3 (c)). In the absence of grain boundaries, there will be no easily activated diffusion mechanisms for N to escape along. Thus, the pseudomorphic growth of CrN will effectively stabilize its composition. Moreover, Mayr et al. [37] showed that nitrogen self-diffusion in CrN_x at 1150 °C and above decreases exponentially with decreasing vacancy concentration. Thus in moving to a less nitrogen-deficient CrN_x ($x<1$) composition during tempering or deposition, a decrease in the diffusion rate can be expected. Thus the stoichiometric-to-overstoichiometric composition in our samples should provide for the most stable nitrogen content during annealing.

During annealing at 900 °C drastic changes of the superlattice structure could be observed. Fig. 6(a) shows the in-situ high temperature XRD intensity of θ–2θ scans covering the CrN/ScN 002 superlattice Bragg-peak as well as the accompanying $n = \pm 1$ superlattice satellites during the annealing at 850 °C and 900 °C. As can be seen, the superlattice remains intact for the entire 26 h period at 850 °C and for additionally

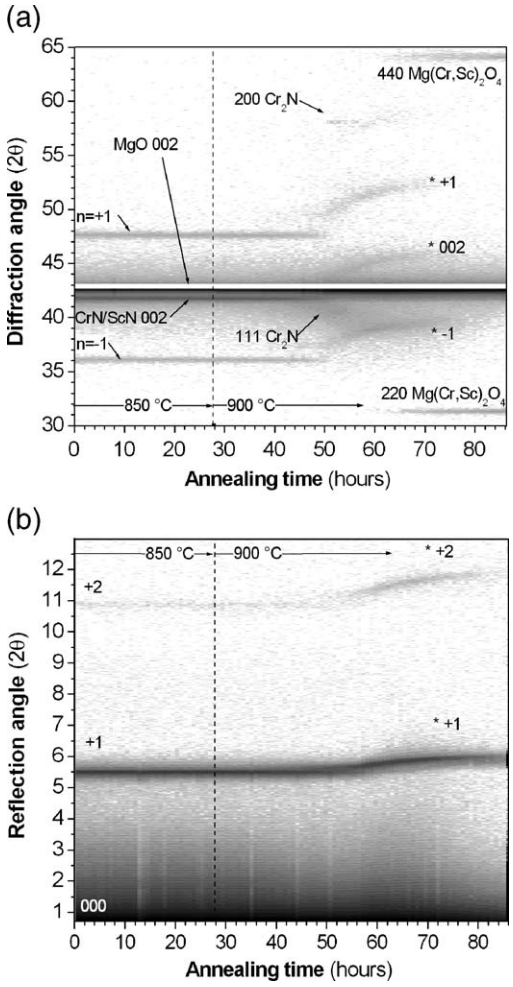

Fig. 6. In-situ high temperature X-ray scattering from a CrN/ScN superlattice grown at 735 °C with a superlattice period Λ of 1.7 nm. (a) XRD covering the CrN/ScN 002 average Bragg peak as well as the $n = \pm 1$ superlattice satellites. The horizontal white band around $2\theta = 43°$ is due to skipping over the MgO 002 substrate peak during the scans. (b) HXR. The figures show the annealing at 850 °C up to 28 h (marked by the dashed vertical line) where the temperature was raised and kept at 900 °C for an additional 58 h. The intensities are mapped on a Log_2 grey-scale map (from white at zero counts/s increasing in 256 levels to black at the maximum intensity) with the temperature along the horizontal axes and the scattering angles along the vertical axes.

20 h annealing into the 900 °C period (46 h at the time axis) where a change of the pattern starts to take place. During a period of 24 h (from 46 to 70 h) the CrN/ScN 002 superlattice Bragg peak as well as the $n=\pm 1$ superlattice satellites make synchronized transitions to higher angles (marked by ∗ in the figure) and the relative intensities of the satellites change drastically with a faint second ($n=+2$) satellite appearing (not marked in the figure). A similar transition of the superlattice reflections is observed in the HXR map shown in Fig. 6(b). These changes correspond to a 7.5% decrease of the average superlattice 002 lattice parameter from $c^{i}=0.4320$ nm to $c^{f}=0.400$ nm and an 8% shrinkage of the superlattice period from $\Lambda^{i}=1.62\pm0.01$ nm to $\Lambda^{f}=1.49\pm0.05$ nm. The similar change in average lattice parameter and superlattice period indicates that a shrinkage of the entire crystal lattice occurred and the alteration of the relative satellite intensities indicate that the relative thicknesses of the CrN and ScN layers also changed during the transition. It is possible to see in Fig. 6 that there is a discontinuity in the change of the CrN/ScN 002 superlattice Bragg peak as well as the $n=\pm 1$ superlattice satellites around 50 h. The changes take a distinct jump when the original superlattice starts to expand. At the same time two small peaks, that can be identified as Cr_2N 111 and Cr_2N 200 (marked in Fig. 6(a)), can be seen in the XRD map of Fig. 6(a) to emerge and vanish around 50 h. Lu and Chen observed that the Cr_2N phase appeared and vanished upon annealing at temperatures between 500 and 700 °C which could be correlated to a relaxation of growth induced stresses [34]. We attribute the observed shrinkage in average CrN/ScN superlattice lattice parameter as well as superlattice period to an out-diffusion of nitrogen from the superlattice as under-stoichiometric transition metal nitrides have been observed have smaller crystal lattices even if they remain in their cubic NaCl structures. However, the discontinuous transition indicate that there is a phase transformation occurring in the cubic superlattice at the same time. At about 62 h, two peaks that can be assigned to be the 220 and 440 reflections of the Mg–Cr–Sc–O spinel phase, $Mg(Cr, Sc)_2O_4$, starts to appear. It is well-known that formation of spinel will occur for transition metal nitrides when they are grown on MgO substrates at temperatures higher than 800–900 °C [38,39]. Here, the spinel formation can be understood from counter-diffusion of the film cations and Mg^{2+} in the rigid oxygen frame provided by the oxygen anion sublattice of MgO. The formation of the spinel is by topotaxial growth with a coherency to the lattices of all the phases involved. The spinel is thus formed by solid state reaction via diffusion. Thus, this observation gives a measure for the temperature where thermal activation of Sc diffusion in ScN as the metal has to leave those layers in order to reach the MgO and form the spinel formation. The nitrogen excess in the superlattice film resulting from the out diffusion of Cr and or Sc can easily be absorbed by the CrN_x layers to balance the stoichiometry away from the film/substrate interface. It is important to note that the initial transformation of the superlattice occurs 12 h before the spinel can be seen which supports the conclusion that a N-out diffusion forego the activation of metal diffusion across the superlattice layers such that Sc and Cr can reach the substrate and form spinel. Thus, the high thermal stability of primarily the ScN layers, but possibly also over-stoichiometric CrN layers, act to hinder diffusion of metal as well as nitrogen. Once the spinel has started to form the spinel peaks are seen to grow stronger during a period of 8–10 h while the superlattice peaks diminish to zero as seen in the XRD map of Fig. 6(a). However, in the HXR map of Fig. 6(b), both the $n=1$ and $n=2$ reflections from the superlattice can be seen, even after 86 h, indicating that some of the transformed super structure still remains.

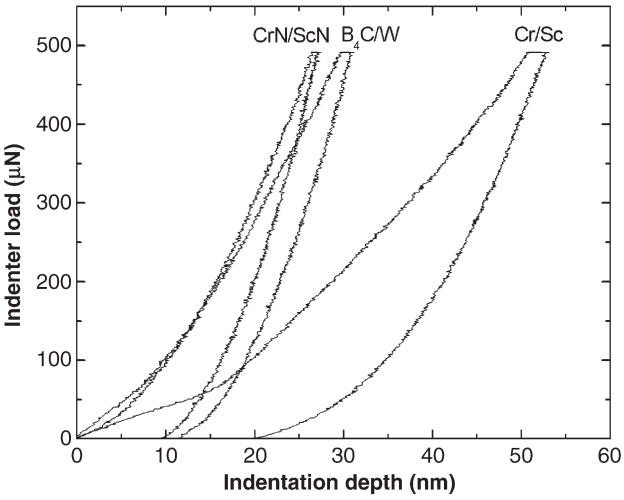

Fig. 7. Load–displacement curves from the nanoindentation experiments on 1 μm thick epitaxial CrN/ScN superlattice films on MgO grown according to the optimal growth process determined in this work. As comparison, load–displacement curves for a 1 μm thick state-of-the-art Cr/Sc X-ray multilayer mirror as well as a 0.34 μm thick B_4C/W X-ray multilayer mirror, both on monocrystalline Si-substrates.

An important property of X-ray mirrors operating in harsh environments is their mechanical stability. In order to investigate this property we measured load–displacement curves by nano-indentation on one superlattice grown to a thickness of 1 μm. As references, we also measured a 1 μm thick multilayer mirror of metallic Cr/Sc which is state-of-the-art in soft X-ray reflectivity (>20%) and a 0.34 μm thick ceramic B_4C/W mirror (thermally stable up to 650 °C), both optimized for the same X-ray energy as the CrN/ScN superlattice, thus having the same bilayer thickness of 1.7 nm. All mirrors were synthesized in our laboratory [2,31,40]. The results are shown in Fig. 7 where it can be seen that the CrN/ScN superlattice has the lowest indentation depth and thus indeed is the hardest of the three. The hardnesses H and Young's modulii E, as determined from the nanoindentation curves, were $H_{CrN/ScN}=19$ GPa and $E_{CrN/ScN}=318$ GPa, $H_{B4C/W}=14$ GPa and $E_{B4C/W}=261$ GPa, and $H_{Cr/Sc}=5$ GPa, and $E_{Cr/Sc}=104$ GPa. The mechanical hardness of the superlattice mirrors are almost as hard as TiN (001) single crystal films which, grown under similar conditions, exhibits a hardness of 21 GPa [13].

4. Conclusion

A process window for synthesis of (001)-oriented CrN/ScN has been found despite the incompatible thermal properties of

the constituting nitrides in their bulk form. Extreme fluxes of very low energy nitrogen ions towards the growing film surface allowed the growth of highly ordered superlattices with modulation periods $\Lambda = 1.7$ nm and interface widths of only one monolayer. We conclude that the successful synthesis is due to a combined effect of three different factors: First, a high flux of low energy ions provides for N activation in the nitride formation and recoil implantation of N to compensate for the concurrent N_2 desorption from the film surface during deposition. Second, the successive layering of CrN and ScN layers in the form of a superlattice supplies both a capping layer (ScN) to act as a diffusion barrier against N loss from the CrN that is unstable at stoichiometric composition at these temperatures and a buffer layer (CrN) to accommodate any trapped N in otherwise over-stoichiometric ScN layers. Third, the coherency strain from the pseudomorphic growth of the two nitrides in the form of a superlattice will fixate the N sublattice.

The single crystal CrN/ScN superlattice mirrors exhibit similar near-normal reflectance as the well known metallic Cr/Sc multilayer system which currently is the state-of-the-art. Moreover, the thermal stability up to 850 °C of the superlattice mirrors in combination with the very high mechanical hardness make them very suited for extreme environments where they can be subject to extensive heat loads or mechanical wear, such as first mirror in the optical path of free-electron lasers, instrumentation based on laser plasma X-ray sources, or in windowless space borne telescopes. The CrN/ScN superlattices have mechanical properties similar to TiN which is industrially used as a protective coating of high performance for metal machining cutting tools, however, its superior thermal stability may prove this superlattice system useful also as high temperature wear protective industrial coating.

Acknowledgements

The authors appreciate the support given by the Swedish Research Council (VR) as well as the Swedish Foundation for Strategic Research (SSF) for their financial support. We would also like to express our thanks to: Dr. F. Schäfers for helping with the soft X-ray measurements at BESSY, Berlin, Dr. D. Music for helping with the nano-indentation measurements, and Dr. U. Kreissig at Forschungzentrum Rossendorf for guidance during the ERDA measurements.

References

[1] F. Eriksson, G.A. Johansson, H.M. Hertz, J. Birch, Opt. Eng. 41 (2002) 2903.
[2] F. Eriksson, G.A. Johansson, H.M. Hertz, E.M. Gullikson, U. Kreissig, J. Birch, Opt. Lett. 28 (2004) 2494.
[3] F. Schäfers, M. Mertin, D. Abramsohn, A. Gaupp, H.-Ch. Mertins, N.N. Salashenko, Nucl. Instrum. Methods A 467/468 (2001) 349.
[4] F. Schäfers, H.-C. Mertins, F. Schmolla, I. Packe, N.N. Salaschenko, E.A. Shamov, Appl. Opt. 37 (1998) 719.
[5] T. Kuhlmann, S. Yulin, T. Feigl, N. Kaiser, T. Gorelik, U. Kauser, W. Richter, Appl. Opt. 41 (2002) 2048.
[6] D.L. Windt, S. Donguy, J. Seely, B. Kjornrattanawanich, E.M. Gullikson, C.C. Walton, L. Golub, E. DeLuca, Proc. SPIE 5168 (2003) 1.
[7] S.A. Yulin, T. Kuhlmann, T. Feigl, N. Kaiser, Proc. SPIE 4782 (2002) 285.
[8] S.A. Barnett, Physics in Thin Films, Academic Press, New York, 1992; L. Hultman, Hard Nanostructured Coatings, Plenum Press, New York, 2005.
[9] U. Helmersson, S. Todorova, S.A. Barnett, J.-E. Sundgren, L.C. Markert, J.E. Greene, J. Appl. Phys. 62 (1987) 481.
[10] M. Shinn, L. Hultman, S.A. Barnett, J. Mater. Res. 7 (1992) 901.
[11] L. Hultman, C. Engström, M. Odén, Surf. Coat. Technol. 133/134 (2000) 227.
[12] D. Gall, I. Petrov, N. Hellgren, L. Hultman, J.-E. Sundgren, J.E. Greene, J. Appl. Phys. 84 (1998) 6034.
[13] H. Ljungcrantz, M. Oden, L. Hultman, J.E. Greene, J.-E. Sundgren, J. Appl. Phys. 80 (1996) 6725.
[14] D. Gall, M. Stadele, K. Järrendahl, I. Petrov, P. Desjardins, R.T. Haasch, T.-Y. Lee, J.E. Greene, Phys. Rev., B 63 (2001) 1251191.
[15] D. Gall, C.-S. Shin, T. Spila, M. Oden, M.J.H. Senna, J.E. Greene, I. Petrov, J. Appl. Phys. 91 (2002) 3589.
[16] D. Gall, C.-S. Shin, R.T. Haasch, I. Petrov, J.E. Greene, J. Appl. Phys. 91 (2002) 5882.
[17] D. Gall, I. Petrov, P. Desjardins, J.E. Greene, J. Appl. Phys. 86 (1999) 5524.
[18] H. Al-Brithen, A.R. Smith, Appl. Phys. Lett. 77 (2000) 2485.
[19] A.R. Smith, H.A.L. Al-Brithen, D.C. Ingram, J. Appl. Phys. 90 (2001) 1809.
[20] K. Inumaru, H. Okamoto, S. Yamanaka, J. Cryst. Growth 237/239 (2002) 2050.
[21] J. Almer, M. Odén, L. Hultman, G. Håkansson, J. Vac. Sci. Technol., A, Vac. Surf. Films 18 (2000) 121.
[22] E.B. Svedberg, J. Birch, I.P. Ivanov, P. Münger, J.-E. Sundgren, J. Vac. Sci. Technol., A, Vac. Surf. Films 16 (1998) 633.
[23] B. Window, N. Savvides, J. Vac. Sci. Technol., A, Vac. Surf. Films 4 (1986) 196.
[24] B. Window, N. Savvides, J. Vac. Sci. Technol., A, Vac. Surf. Films 4 (1986) 453.
[25] C. Engström, T. Berlind, J. Birch, L. Hultman, I.P. Ivanov, S.R. Kirkpatrick, S. Rohde, Vacuum 56 (2000) 107.
[26] D.K.G. de Boer, A.J.G. Leenaers, Physica B 221 (1996) 18.
[27] J.R. Tesmer, M. Nastasi, Handbook of Modern Ion Beam Materials Analysis, Materials Research Society, Pittsburgh, 1995.
[28] W.C. Oliver, G.M. Pharr, J. Mater. Res. 7 (1992) 1564.
[29] I. Petrov, A. Meyrs, J.E. Greene, J.R. Abelson, J. Vac. Sci. Technol., A, Vac. Surf. Films 12 (1994) 2846.
[30] F. Eriksson, F. Schäfers, E.M. Gullikson, S. Aouadi, N. Ghafoor, S. Rhode, L. Hultman, J. Birch, PhD Thesis by F. Eriksson, Linköping Studies in Science and Technology No. 875, Linköping University, Sweden, 2004.
[31] F. Eriksson, N. Ghafoor, F. Schäfers, E.M. Gullikson, J. Birch, PhD Thesis by F. Eriksson, Linköping Studies in Science and Technology No. 875, Linköping University, Sweden, 2004.
[32] D.L. Windt, Comput. Phys. 12 (1998) 360.
[33] B.L. Henke, E.M. Gullikson, J. Davis, Atomic Data and Nuclear Data Tables, 1993.
[34] F.-H. Lu, H.-Y. Chen, Thin Solid Films 398/399 (2001) 368.
[35] W. Herr, E. Broszeit, Surf. Coat. Technol. 97 (1997) 335.
[36] P.H. Mayrhofer, G. Tischler, C. Mitterer, Surf. Coat. Technol. 142/144 (2001) 78.
[37] W. Mayr, W. Lengauer, P. Ettmayer, D. Rafaja, J. Bauer, M. Bohn, J. Phase Equilib. 20 (1999) 1.
[38] L. Hultman, J.-E. Sundgren, D. Hesse, J. Mater. Res. 4 (1989).
[39] L. Hultman, D. Hesse, W.-A. Chiou, J. Mater. Res. 6 (1991).
[40] F. Eriksson, PhD Thesis, Linköping Studies in Science and Technology No. 875, Linköping University, Sweden, 2004.